Proceedings of the Institution of Mechanical Engineers, Part B: Journal of Engineering Manufacture

Monitoring and processing the acoustic emission signals from the friction-stir-welding process

V Soundararajan, H Atharifar and R Kovacevic

The online version of this article can be found at:

Published by:

⑤SAGE

http://www.sagepublications.com

On behalf of:

Institution of MECHANICAL ENGINEERS

Institution of Mechanical Engineers

Additional services and information for *Proceedings of the Institution of Mechanical Engineers, Part B: Journal of Engineering Manufacture* can be found at:

Email Alerts: http://pib.sagepub.com/cgi/alerts

Subscriptions: http://pib.sagepub.com/subscriptions

Reprints: http://www.sagepub.com/journalsReprints.nav

Permissions: http://www.sagepub.com/journalsPermissions.nav

Citations: http://pib.sagepub.com/content/220/10/1673.refs.html

>> Version of Record - Oct 1, 2006

What is This?

Monitoring and processing the acoustic emission signals from the friction-stir-welding process

V Soundararajan, H Atharifar, and **R Kovacevic***
Department of Mechanical Engineering, Southern Methodist University, Richardson, Texas, USA

Abstract: This paper discusses the detection and analysis of the acoustic emission (AE) signals to investigate the possibility of applying the AE technique for the in-process monitoring of the friction-stir-welding process. Tests are carried out for joining similar and dissimilar metals using a high-speed rotating tool under various rotational speeds and traverse speeds and for different tool penetration depths. The results of fast Fourier transform show that the amplitude of the AE signal in the frequency domain is sensitive to the change in the depth of penetration of the tool. Signals in certain frequency ranges disappear when the tool loses contact with the workpiece during the process. Discrete wavelet transform indicates significant sudden changes in the decomposed signal in the lower frequency ranges (higher levels) when the shoulder makes contact with or detaches itself from the workpieces. By identifying the frequencies during the process and analysing the wavelet decomposed signals in various levels or frequency bands, it is possible to monitor effectively the transient welding state and to identify quickly 2the process changes.

Keywords: acoustic emission, fast Fourier transform, power spectrum, short-time Fourier transform, discrete wavelet transform, continuous wavelet transform, friction stir welding, process monitoring

1 INTRODUCTION

Friction stir welding (FSW) is a solid-state joining process where heat is generated when a rotating tool plunges into the workpiece and its shoulder comes into contact with the workpiece, resulting in a thermomechanical state that is conducive for material flow and weld formation. Because the material offers resistance to the tool plunge, an equilibrium steady state is attained after the start of the process at a certain depth of penetration of tool into the workpieces. This novel joining technique, which was initially applied for joining aluminium alloys, has now rapidly expanded its applications to join steel and titanium alloys [1, 2]. Because of this, monitoring of the weld quality and welding process has become more important in recent years. In order to automate this process and to make it more efficient, it must incorporate a technique for in-process monitoring of the tool condition and the weld formation [3].

Acoustic emission (AE) monitoring is widely used for real-time detection of the cutting tool wear [4, 5] and for estimating the workpiece quality [6]. Chen *et al.* [3] discussed AE-based monitoring of the FSW process. They mentioned that the fast Fourier transform (FFT) method is not appropriate for the present case as the signal is time variant. Their research focused on the investigation of AE signals using wavelet transforms by having abrupt changes in the workpiece geometry. Finally, they concluded that the different types of defect yield different features in a specific range of frequencies and the band energy variation can provide an indication of gap-induced defects. Chen *et al.* [3] also mentioned that the largest problem in using AE to monitor FSW is that a large number of components are involved in generating the AE signals, making it very difficult to extract the valuable features from the AE signals.

*Corresponding author: Department of Mechanical Engineering, Southern Methodist University, Research Centre for Advanced Manufacturing, 1500 International Parkway, Suite no. 100, Richardson, TX 75081, USA. email: kovacevi@engr.smu.edu

The signals acquired during FSW are found to be time variant in the plunge phase but produce a steady power spectrum during the welding process. In this paper, the signals acquired for different process parameters during the steady state of the process and also the signals obtained by abruptly changing the parameters during the process are discussed. The informative features of the signal related to the tool interaction with the workpiece and the welding state are studied using the FFT, the short-time Fourier transform (STFT) and the discrete wavelet transform (DWT). It is difficult to correlate the frequency of the signal directly to various interactions that occur during the process, but loss of contact between the tool and workpiece stands out. The frequencies produced in a certain range disappear immediately when this contact is lost. This research will finally focus on showing the effect of tool plunge depth increase on the acquired signals.

2 THEORETICAL BACKGROUND

AE signals are sound waves generated and propagated in solid media. Generally, this signal is affected by the characteristics of the source, the sensor, the wave-travelling path, and the data acquisition system. Therefore, it is intricate dealing with this kind of signal and extracting the required information from the raw data. Many methods are introduced to tackle this problem, ranging from simple waveform parameter measurement in experimental tests to pattern recognition approaches in online monitoring of the complex systems. The most important signal-processing approaches used for extracting useful information from an AE signal can be categorized as follows.

2.1 Fast Fourier transform

This method is used to represent the frequency response of a system. The FFT method has the capability to decompose the different frequencies in the original signal that are related to different sources. The Fourier transform of an energy-limited signal $x(n)$ can be written typically as

$$x(n) = \frac{1}{2\pi} \int_{-\infty}^{\infty} X(\omega)\, e^{j\omega n}\, d\omega \qquad (1)$$

where

$$X(\omega) = \sum_{n=-\infty}^{\infty} x(n)\, e^{-j\omega n} \qquad (2)$$

Equation (1) represents the decomposition of the input signal $x(n)$ to a series with weighting coefficient $X(\omega)$ for each harmonic of $e^{j\omega n}$. Equation

(2) is independent of time, showing the composition of the frequencies for the stationary signal $x(n)$.

In this paper, the capability of the FFT method to explain the lack of contact between the shoulder and the workpieces will be represented. Since the results are the frequencies averaged over the duration of the signal, the FFT cannot adequately describe the characteristics of the AE signal at lower frequencies. Therefore, other signal-processing techniques are utilized to characterize the AE signal over frequency ranges. FFT transformation plots with the power spectrum over the discretized frequencies of signal is the most commonly used tool to reveal the power consumption pattern. Assuming the AE signal to be $x(t)$, the power spectrum density (PSD) of a stationary process is defined as [7]

$$P_{xx}(\omega) = \sum_{n=-\infty}^{\infty} r_{xx}(t)\, e^{-j2\pi\omega t}, \qquad n, t \in Z \qquad (3)$$

where

$$r_{xx}(t) = E[x(t)x(t+k)], \qquad k \in Z \qquad (4)$$

For transient signals, a short time window is usually applied to filter the signals, resulting in the so-called spectrogram. However, for high time-variant signals, the spectrogram may not be sufficiently suitable since its accuracy for extracting the frequency information is limited by the window length. So, in this research the qualitative value of power spectrum density will be important when comparing the results of different experiments.

2.2 Short-time Fourier transform

In an effort to correct the deficiency of the FFT method, the STFT or Gabor transform was introduced adapting the Fourier transform to analyse only a small section of the signal at a time (windowing). The spectral coefficients are calculated for this short length of data; then the small section is moved to a new position and the calculation is repeated. This method maps a signal into a two-dimensional function of time and frequency and has diverse application in the signal-processing area, especially for the AE signals [8]. The formulation introduced by Gabor assuming the energy limited signal of $x(n)$ with a Gaussian window can be expressed as

$$X_{STFT}(\omega, T) = \int_{-\infty}^{\infty} x(t)W(t-T)\, e^{-j\omega t}\, dt \qquad (5)$$

In equation (5), W is called the window function with a time duration T. The spectral coefficients will be calculated assuming the same time duration or the frequency bandwidth $1/T$. The STFT plots of a signal represent a compromise between the

time- and frequency-based views of a signal. It gives some information about the time and the frequency at which a signal event occurs which is of limited precision determined by the size of the window. While the STFT compromise between time and frequency information can be useful, the drawback is that there are the same sizes of window for all frequencies for a particular duration of time.

2.3 Wavelet transform

The basic idea behind wavelet-based analysis is to describe the non-stationary signal in a two-dimensional space of timescale. Wavelet analysis represents the windowing technique with regions of various sizes. Wavelet transform allows the use of long time intervals where more precise low-frequency information is required, and shorter regions where high-frequency information is needed. It has a wide variety of applications in signal processing mainly owing to the outstanding localization property [**9**, **10**]. For a given wavelet function of $\psi(t) \in L^2(R)$, where $L^2(R)$ is the set of signals with finite energy, the signal $x(t)$ can be decomposed using continuous wavelet transform with the equation given by

$$C_{a,b}(x) = |a_0|^{-0.5} \int_{-\infty}^{\infty} x(t)\bar{\psi}\left(\frac{t-b}{a}\right) \mathrm{d}t, \quad a,b \in R, \quad a \neq 0 \tag{6}$$

where a_0 is the normalization factor and $\overline{\psi}$ is the conjugate function of $\psi(t)$ with the scale parameter a and shift value b.

For each given scale a, the wavelet coefficients $C_{a,b}$ for $b = 1$ correspond to a length of signal $x(t)$. $C_{a,b}$ is a real or complex matrix depending on the wavelet type. From equation (6), it is obvious that the matrix $C_{a,b}$ will have numerous data stored and, in most practical issues, some specific frequency bands that are important to study. So, if the scales and positions are based on powers of two, the analysis will be much more efficient. In 1989, Mallat [**11**] introduced a fast wavelet decomposition and reconstruction algorithm that is classically called DWT. The idea was to develop a practical filtering algorithm that yields fast wavelet transform. The algorithm is well known as a two-channel subband coder using conjugate quadrature filters or quadrature mirror filters. It looks like a box into which a signal passes, and out of which wavelet coefficients quickly emerge. In DWT, the scale parameter a and position parameter b can be written as

$$a = 2^j, \quad b = k2^j, \quad (j,k) \in Z^2 \tag{7}$$

As mentioned before, the ultimate goal in wavelet transform is to decompose the original
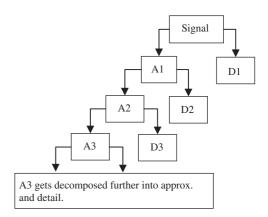

Fig. 1 Wavelet decomposition tree showing approximations and details of signal for three levels

signal into a series of approximations (labelled A) and details (labelled D) distributed over different frequency bands, preserving the characteristics of the time domain and frequency domain. The decomposition tree is shown schematically in Fig. 1. The characteristics of frequency and time are preserved simultaneously in this decomposition and the frequency band of approximation and detail for a level l are $[0, 1/2f2^{-1}]$ and $[1/2f2^{-1}, 1/2f2^{-(l-1)}]$

Integration of the wavelet signals over time yields the wavelet energy contained at a particular time-scale. Such scales carry maximum information about the process under analysis and they should be studied more carefully. On the other hand, the scales with smaller values of energy contain virtually no useful information and can be excluded from consideration. The wavelet energy is given by

$$\mathrm{Energy}(a) = \frac{1}{N}\sum_{b=1}^{N} C_{a,b}^2 \tag{8}$$

where N is the number of sample points in time and $C_{a,b}$ is the wavelet coefficient.

3 EXPERIMENTAL SET-UP AND PROCEDURE

An adapted automatic computer numerically controlled milling machine was used for FSW (Fig. 2). It provides a wide range of rotational and traverse speeds, and the depth of penetration for the welding of the workpieces. The workpieces, 6 mm thick, 200 mm long, and 50 mm wide, are friction stir welded along the butted joint. The tool is made from CPM-1V tool steel and consists of a shoulder of 24 mm diameter and a pin of 6 mm diameter and 5.5 mm height.

An online AE monitoring system was used to detect the welding state and to evaluate the weld quality during the probe penetration, welding,
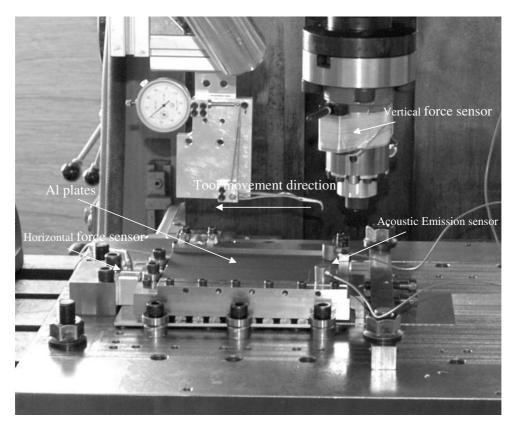
Fig. 2   Fixture for FSW with AE sensors

and pin pull-out. The two AE sensors are arranged symmetrically on both sides of the butting joint of the parts with a distance of 70 mm to the butting line and mounted on the top surface of the workpiece. A couplant is used to provide a good acoustic path between the workpiece and the sensor.

AE sensing is based mostly on processing signals with a frequency range from 10 kHz to about 800 kHz for machining processes with cutting operations [12]. From the preliminary studies, the frequency range for the FSW process is between 100 and 300 kHz. Before the start of the process, the AE test results recorded on the butted plates with the machine in the running mode were found to contain noises due to machine vibration at amplitudes below 45 dB. In order to filter out the mechanical noise, a bandpass filter was used for collecting signals in the range 10–400 kHz during the FSW process. The AE signal data from the two sensors (channel 1 and channel 2) were found to have the same frequency and amplitude response by calibration. The AE data generated during welding were collected for the entire welding process, progressively amplified through the preamplifier with a 40 dB gain, passed through the 10–400 kHz bandpass filter to filter out the low-frequency noise, and transmitted to the signal processor, as shown in Fig. 3. The AE voltage output was sampled by the MISTRAS data acquisition system at a rate of 1 MSPS (million samples per second).

Three experiments were conducted joining the aluminium alloy 6061 workpieces. Experiment 1 involved variation in the rotational speed of the tool, in three stages: 500, 750, and 1000 r/min. During experiment 2, the welding speed and rotational speed used during the first half of the process, which had been maintained at 75 mm/min and 400 r/min respectively, were suddenly changed in the second half of the weld to 50 mm/min and 750 r/min respectively. The objective of experiment 2 was to observe the change in the AE signal due to the drastic variation in the thermomechanical condition that exists in the weld zone. In experiment 3, the depth of penetration was increased from 0.2 mm initially to 0.4 mm and then further to 0.6 mm. The contact between the tool shoulder and the workpiece is not properly established initially, but a very good contact condition is obtained in the later two stages of the process. The welds obtained under the various process parameters are shown in Fig. 4.

4   RESULTS AND DISCUSSION

4.1   AE signal from the FSW process

As mentioned in section 3, the acquired AE data are amplified and passed through a bandpass filtering system to allow the specific amplitudes of AE data
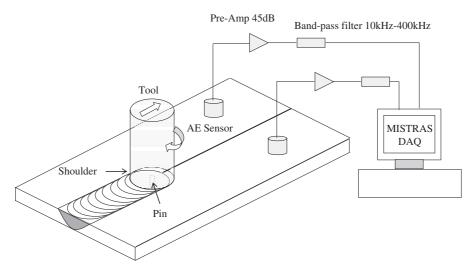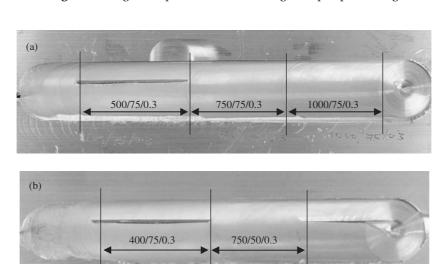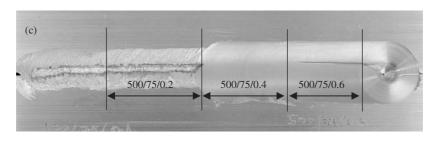
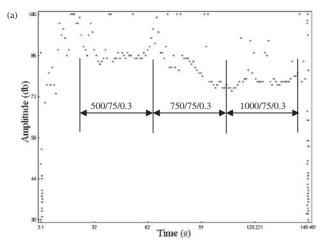**Fig. 3** AE signal acquisition, conditioning, and pre-processing
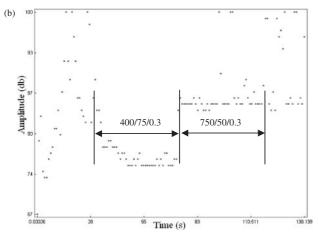

Direction of welding

Fig. 4 Top view of the friction stir welds shown after (a) experiment 1, (b) experiment 2, and (c) experiment 3 (AE signals acquired along the marked regions are actively considered for analysis). 500/75/0.3 means a rotational speed of 500 r/min, a traverse speed (welding speed) of 75 mm/min and a depth of penetration of 0.3 mm into the workpiece

to be recorded. Generally, AE signals are one of two distinct kinds: the continuous AE signal that arrives at the transducer in large numbers wh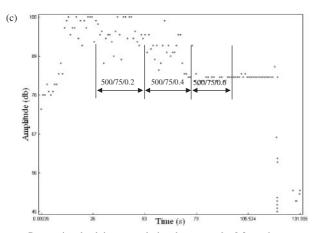en distinct events cannot be observed, and the impulsive signals that distinguish the AE events. AE signals are transient elastic waves propagated through the solid media during the operation of FSW. The AE signal will be detected by the sensor when a distinct

(a)

Tool rotational speed changes in three stages

(b)

Tool rotational speed and feed rate changes in two stages

(c)

Penetration depth increases during the process by 0.2 mm in two stages

Fig. 5 Accumulation of hits detected using the AE sensor in FSW for different process parameters

wave has the capability to pass the filtering system. Figure 5 shows the recorded waves (also known as hits) over time in the different experimental conditions shown in Fig. 4. The spread of these hits explicitly demonstrate the change in the amplitude of the waves when the process parameters change. Each hit observed in Fig. 5 happens in a specific

time duration during which the process contains a distinct discrete-time signal with the amplitude of the voltage over time.

Figure 5 shows how the amplitude of the recorded hits varies with the changing rotational speed, feed rate, and penetration depth of the tool. The difference between the amplitude of hits mainly depends on the thermomechanical conditions in the welding zone, which change dramatically with temperature and stress. An increase in the rotational speed changes the heat input to the welding zone, resulting in an increase in the shear rate of the workpiece in the thermomechanically affected zone (TMAZ). An increase in the feed rate, on the other hand, decreases the heat input and leads to cutting of the material rather than plastic flow of the material around the tool pin. Lack of proper contact between the tool shoulder and the workpiece leads to insufficient heat for plasticizing the underlying material. The penetration depth parameter ensures this contact during the FSW process. A large penetration depth leads to greater stress in the TMAZ and surface void generation.

Figure 5(a) shows the effect of the rotational speed on the amplitude of hits obtained from AE sensors. It is obvious that rotational speed change does not have a major impact on the amplitude during the process. Figure 5(b) represents the drastic change in the process parameters on the signal amplitudes. This change clearly produces a shift in the amplitude range. In Fig. 5(c), initially there is lack of contact between the tool and workpiece, producing a signal with random amplitudes. However, once the contact is established, the amplitude range becomes uniform.

Cumulatively, Fig. 5 helps the qualitative changes in amplitude of the AE hits when the material properties change drastically because of the varying thermomechanical and contact conditions in the FSW process to be understood.

4.2 Processing the AE signal

4.2.1 Study of the effects of the changes in the rotational speed and the welding speed on the AE signal

Experiment 1 involved an increase in the rotational speed of the tool in three stages while maintaining the welding speed and the depth of penetration constant during the entire process. Many workers [8, 13] have discussed the direct quantitative relationship between the heat generated and the tool rotational speed. As the speed increases, the material in the weld zone, TMAZ, and the heat-affected zone starts to plasticize, further leading to an increase in the actual depth of penetration and a decrease in the interaction force between the tool and the
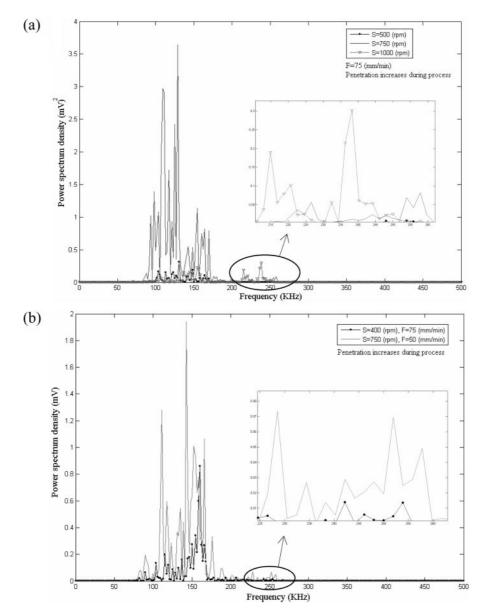
Fig. 6 PSD versus frequency plots for different process parameters: (a) experiment 1; (b) experiment 2

workpiece. It has been observed that only under the existence of certain thermomechanical conditions will weld formation without a void be successful [**14**, **15**].

From the qualitative observation of the weld in experiment 1 (Fig. 4), the following can be summarized. For a rotational speed of 500 r/min, there is surface void formation, indicating lack of proper contact between the shoulder and workpiece. For a rotational speed of 750 r/min, a good weld with no defect is formed. For a rotational speed of 1000 r/min, there is an internal defect, indicating that excessive heat has caused the aluminium to fluidize greatly, leading to the generation of the void at the interface of the TMAZ and the weld nugget.

Figure 6 shows the FFT of the AE signal for different process parameters. The frequencies of the AE signal from the FSW process lie in the ranges 100–170 kHz and 215–260 kHz. The PSD in Fig. 6(a) for experiment 1 shows that it increases as the rotational speed increases from 500 to 750 r/min but lies mainly in the frequency range 100–170 kHz, explaining that the effect of better contact between the shoulder and the workpiece leads to an increase in the PSD without any major change in the frequency range of the signal. However, during the change in the rotational speed from 750 to 1000 r/min, it could be seen that the values of the PSD decrease in the region of 100–170 kHz but increase in the region of 220–260 kHz. This may be explained by the fact that, as the temperature of the workpiece material comes closer to its melting point, the material resistance to the tool becomes negligible and the material flows without resistance
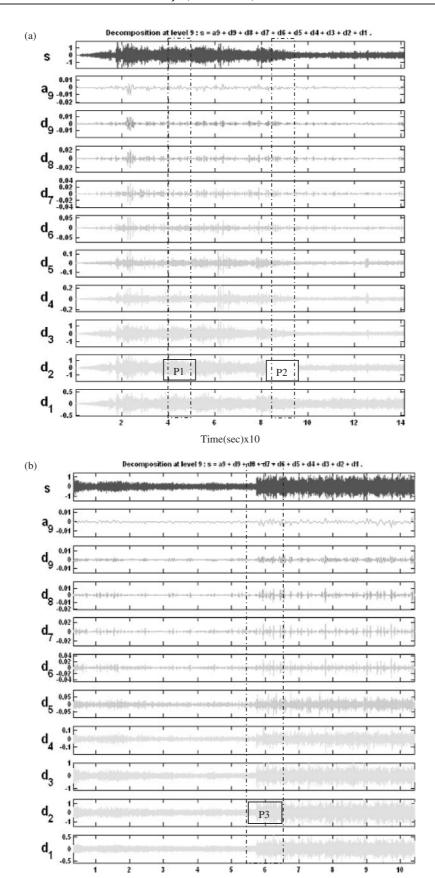
Fig. 7 DWT results depicting changes in the FSW parameters for (a) experiment 1 and (b) experiment 2
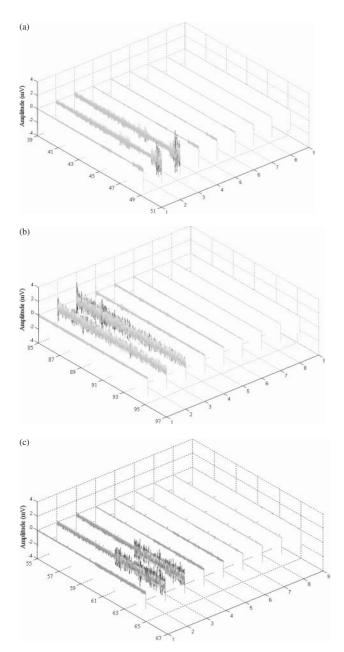
(a)

(b)

(c)

Fig. 8 Three-dimensional plots of zoomed DWTs for sudden changes in parameter for (a) experiment 1, P1 (40–50 s), (b) experiment 1, P2 (85–95 s), and (c) experiment 2, (55–65 s)

around the tool pin. This leads to AE signals that show up in the higher frequency range.

Figure 6(b) depicts the PSD versus the frequency plot for experiment 2 (Fig. 4) wherein the initial process parameters 400 r/min and 75 mm/min are changed to 750 r/min and 50 mm/min, leading to a steep rise in the temperature input to the workpiece, which in turn induces a very high thermal stress in the weld zone. It can be observed that this change in the process condition leads to a large increase in the PSD in the frequency range 90–170 kHz. The macrosection of the weld shows that initially there is a surface void while, after the change of parameters, a good weld without an internal void is obtained. The PSD of the second case (750 r/min and 50 mm/min) in experiment 2 resembles closely the PSD in the second case (750 r/min and 75 mm/min) in experiment 1.

Figure 6 also shows the various peaks of the PSD, with the highest being at a frequency of 140 kHz. The origin and source of those frequencies with higher PSD could be any noise, any new contact that generates new frictional forces, and a solid or semisolid state of shear. Based on the information on FFT diagrams and without using any other signal-processing technique, the time to the process changes or the particular origin of the various peaks in the PSD cannot be identified.

Figure 7 represents the DWT of the AE signal for experiments 1 and 2. In this figure, the transformation has been carried out up to nine levels. The process parameter changes occur in the zones of P1 and P2 indicated in Fig. 7(a) in time intervals of 40–50 s and 85–95 s respectively. Similarly, the process change occurs in the zone of P3 in Fig. 7(b) in a time interval of 55–65 s.

Level 9 in Fig. 7(a) (experiment 1) shows that changing the rotational speed from 500 to 750 and then to 1000 r/min has eliminated the large fluctuations in signal and made it more stable. There is little resistance offered for the tool pin movement through the workpiece at these rotational speeds. Figure 7(b) shows the reverse trend where a stable
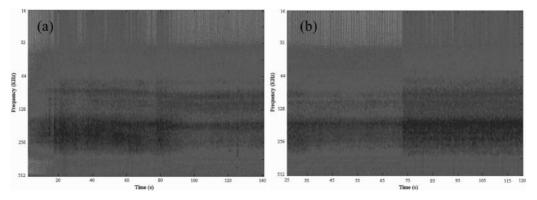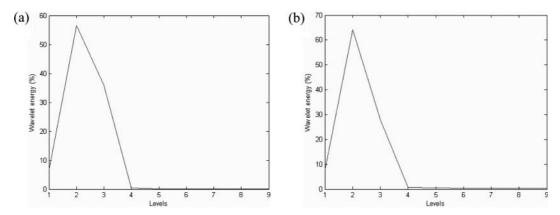
Fig. 9 STFTs of the experiment with changes in the process parameters indicated as darker regions

Fig. 10 Percentage of energy corresponding to the approximation and details for discretized levels in DWT for (a) experiment 1 and (b) experiment 2
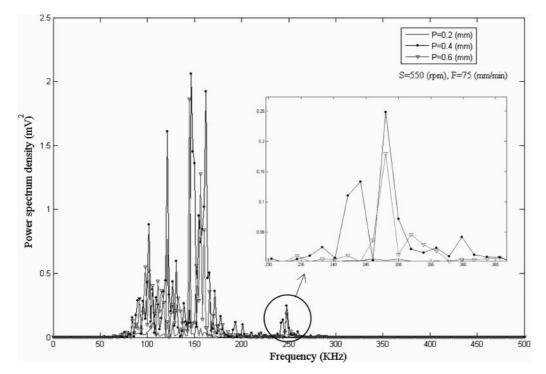

Fig. 11 PSD result for experiment 3

signal at level 9 becomes relatively unstable. This is caused because of the better contact between the shoulder and the workpiece. From this analysis, it can be seen that a stable signal does not necessarily mean that the process is producing a good weld when in fact the indications are the opposite. The centre-line-type rectangles (indicated by regions P1, P2, and P3) drawn in Fig. 7 were used to zoom the specific areas of interest when the process parameter changes suddenly and these are illustrated as three-dimensional plots in Figs 8(a), (b), and (c) respectively, with time-level and amplitude axes.

Figure 9 shows that the AE signals are also analysed with STFT with a plot of frequency versus time. The darker regions in the figure indicate the intensity of the PSD; the darker the region, the stronger is the PSD in the frequency band. A band of darker region exists around the frequency range 100–170 kHz, indicating that most of the AE signal lies in this area. Figure 10 shows the percentages of the wavelet energy at different levels for the entire process in experiments 1 and 2. Higher percentages of energy in levels 2 and 3 indicate that much noise is generated at lower frequencies during the process.

4.2.2 Study of the effect of the penetration depth on the signal

In the experiments discussed in the previous section, it was observed that a distinct frequency range between 220 and 260 kHz existed that did not exhibit a PSD comparable with the frequency band of
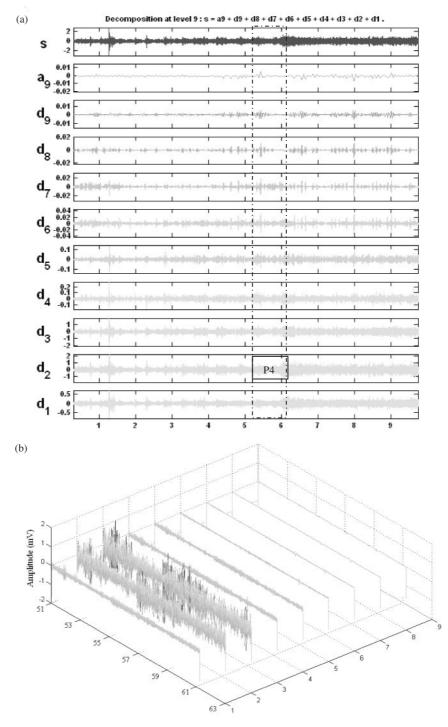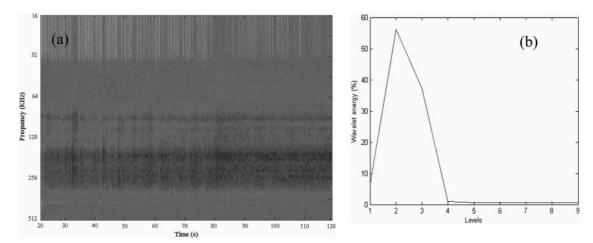
Fig. 12 (a) DWT of the signal from experiment 3 in the time period 50–60 s and (b) its three-dimensional plot

100–170 kHz. In order to study the source of this frequency further, an experiment was performed in which the depth of penetration is intentionally varied during the course of the process. The initial penetration depth of 0.2 mm was increased to 0.4 mm during the process, maintaining the rotation speed as 500 r/min and the welding speed as 75 mm/min. During the first stage of this experiment, there is hardly any contact between the shoulder and the workpiece, indicating that the pin is cutting through the aluminium alloy rather than mixing the weld zone in its plastic state. However, once the depth of penetration is increased to 0.4 mm, very good contact is established between the shoulder and workpiece and the material starts to plasticize from the frictional heat and flow around the pin. Also, the weld is formed without internal or external voids. The penetration depth was then

Fig. 13 (a) STFT results for experiment 3 and (b) the percentage of energy related to the approximation and details in DWT

further increased by 0.2 mm to 0.6 mm. At this stage, the start of void formation in the weld zone was observed.

The FFT results for this experiment are shown in Fig. 11. They indicate that the increase in the penetration depth that leads to the establishment of the contact is the main reason for the appearance of such higher frequencies in the range of 220 and 260 kHz. There is also an appreciable increase in the power spectra and the peaks tend towards 150 kHz from 130 kHz. This clearly shows the possibility of monitoring the loss of shoulder contact with the workpiece.

Figure 12 gives the wavelet decomposition of the signal for experiment 3. The region denoted P4 indicates the time duration when the contact is established by increasing the depth of penetration. The approximation plot from the wavelet decomposition (A9) in this region shows the instability in the signal, indicating a major change in the process, which in the present case occurs during the establishment of the contact.

Figure 13 gives the STFT results and the energy percentage at the different levels for experiment 3. The STFT hardly provides any information other than indicating the development of a darker region during the process after the contact is established in the frequency band 220–260 kHz.

5 CONCLUSIONS

At the end of the initial plunge phase and the start of the welding process, FSW attains a steady state when the thermomechanical conditions in the active welding region remain constant. However, if the process varies in this period, the quality of the weld is affected. AE signals are acquired with different process parameter variations, and signal-processing techniques such as FFT, STFT, and the wavelet transform are used to distinguish these variations as they happen to provide real-time feedback.

There are two distinct frequency ranges observed during the process. The results show that increases in the thermal stress and temperature of the workpiece lead to an increase in the PSD of the signals in the lower-frequency band 100–170 kHz. However, once the temperature increases and nears the melting point of the workpiece, the power spectrum amplifies in the higher-frequency range 220–260 kHz and diminishes in the lower-frequency range 100–170 kHz. The results also show that the signals in the higher-frequency range disappear when the tool loses contact with the workpiece. On decomposing the signals using wavelet transforms, it was observed that a stable process producing good weld results in more fluctuation of the approximated level of the signal in comparison with weld formation with voids. The wavelet transforms also show that a change in the contact condition between the shoulder and workpiece results in a spike in the approximation plot.

The short-time Fourier transforms of the signals are also plotted, but very little information could be gathered from them for monitoring the FSW process. The representations of the wavelet energy signature over the frequency band for different parameters show similar energy levels and the lack of any variation to associate them with the process changes.

Center for Advanced Manufacturing, in preparing the experiments for this research work.

REFERENCES

1 **Lienert, T. J., Stellwag, W. L., Grimmett, B. B.,** and **Warke, R. W.** Friction stir welding studies on mild steel. *Welding J.*, January 2003, **82**(1), 1–9.

2 **Jata, K. V., Subramanian, P. R., Reynolds, A. P., Trapp, T.,** and **Helder, E.** Friction stir welding of titanium alloys for aerospace applications: microstructure and mechanical behavior. In Proceedings of the 14th (2004) International Offshore and Polar Engineering Conference (*ISOPE 2004*) (Toulon, France), 2004, pp. 22–27.

3 **Chen, C., Kovacevic, R.,** and **Jandric, D.** Wavelet transform analysis of acoustic emission in monitoring friction stir welding of 6061 aluminum. *Int. J. Mach. Tools Mf.*, October 2003, **43**(13), 1383–1390.

4 **Tanaka, T.** and **Okitsu, A.** Diagnostic sensing of tool wear by spectrum analysis of interrupted cutting forces. *Bull. Japan Soc. Precision Engng*, 1979, **13**, 45–46.

5 **Matsuoka, K., Forrest, D.,** and **Tse, M. K.** On-line wear monitoring using acoustic emission. *Wear*, 1993, **162–164**, 605–610.

6 **Tönshoff, H. K., Jung, M., Männel, S.,** and **Rietz, W.** Using acoustic emission signals for monitoring of production processes. *Ultrasonics*, 2000, **37**, 681–686.

7 **Vaseghi, S. V.** *Advanced signal processing and digital noise reduction*, 1996 (John Wiley–Teubner Press, West Sussex).

8 **Frigaard, O., Grong, O.,** and **Midling, O. T.** Modeling of the heat flow phenomena in friction stir welding of aluminum alloys. In Proceedings of the Seventh International Conference on *Joints in aluminum* (*INALCO '98*), Cambridge, Massachusetts, USA, 15–17 April 1998, pp. 15–17 (Abington Publishing, Cambridge, UK).

9 **Strang, G.** and **Nguyen, T.** *Wavelets and filter banks*, 1996 (Wellesley–Cambridge Press, Cambridge, Massachusetts).

10 **Wickerhauser, M. V.** *Adapted wavelet analysis from theory to software*, 1994 (Wellesley, Cambridge, Massachusetts).

11 **Mallat, S.** A theory for multiresolution signal decomposition: the wavelet representation. *IEEE Pattern Analysis Mach. Intell.*, 1989, **11**(7), 674–693.

12 **XiaoQi, C., Hao, Z.,** and **Wildermuth, D.** In-process tool monitoring through acoustic emission sensing. SIMTech Technical Report AT/01/014/AMP, 2001, Automated Materials Processing Group, Singapore Institute of Technology.

13 **Soundararajan, V., Zekovic., S.,** and **Kovacevic, R.** Thermo-mechanical model with adaptive boundary conditions for friction stir welding of Al 6061. *Int. J. Mach. Tools Mf.*, November 2005, **45**(14), 1577–1587.

14 **Schmidt, H.** and **Hattel, J.** A local model for the thermomechanical conditions in friction stir welding. *Modelling Simulation Mater. Sci. Engng*, 2004, **13**, 77–93.

15 **Soundararajan, V.** and **Kovacevic, R.** Simulation of temperature field in friction stir welding using material behavior and deformation analysis. In *Contemporary achievements in mechanics, manufacturing and materials science*, Poland, December 2005.

APPENDIX

Notation

a	scale parameter (each scale represents a frequency)
a_0	normalization factor
A1–A9	approximation levels (low-pass filters)
b	shift value or position parameter in time
$C_{a,b}(x)$	wavelet coefficients for the signal $x(t)$
D1–D9	detail levels (high-pass filters)
$e^{j\omega n}$	harmonics in the fast Fourier transform
$E[x(t)]$	energy of signal $x(t)$
Energy (a)	band energy corresponding to scale a
f	frequency of the signal (kHz)
l	level of wavelet decomposition
$P_{xx}(\omega)$	power spectrum density
r_{xx}	autocorrelation for the digital input signal of $x(n)$
t	time (s)
$W(t - T)$	window function for time duration T in the short-time Fourier transform
$x(n)$	energy-limited digital signal
$x(t)$	acoustic emission signal function of time
$X(\omega)$	weighting coefficient for the fast Fourier transform
$\psi(t)$	wavelet function
$\overline{\psi}(t)$	conjugate wavelet function